

O + C_nH_{2n} Products Detected via IR Emission. 1. O + C₂H₄James A. Dodd,* Eunsook S. Hwang,[†] Karen J. Castle,[‡] and Gary D. DeBoer[§]Air Force Research Laboratory, Space Vehicles Directorate,
Hanscom Air Force Base, Massachusetts 01731-3010

Received: June 21, 2004; In Final Form: August 31, 2004

20060203 068

DTIC COPY

Collisions between oxygen atoms and ethene have been investigated by using infrared emission detection of the chemiluminescent product species. A prototypical alkene, ethene, nonetheless exhibits numerous reaction pathways in reactions with O atoms. Oxygen atoms were formed via photolysis of SO₂ in the presence of C₂H₄, and the resultant IR emissions in the 900–3000-cm⁻¹ spectral region were detected by using a time-resolved, step-scan Fourier transform spectrometer. A Welsh cell mirror arrangement was used to maximize the collection efficiency of the product IR emissions. Vibrationally excited products such as CO, CO₂, HCO, and H₂CO have been identified, with CO and CO₂ being the dominant IR emitters. The time-evolving CO and CO₂ spectra have been characterized with respect to the SO₂ and C₂H₄ partial pressures and laser fluence. The rate constants for vibrational relaxation of CO₂ high-*v* population by C_nH_{2n} (*n* = 2–4) are in the mid-10⁻¹² cm³ s⁻¹ range; SO₂ is a very inefficient relaxer. A chemical kinetics code has been used to model the chemistry and identify the operative reaction mechanisms, including the effects of secondary chemistry.

1. Introduction

Hydrocarbons are not present to any significant extent in the Earth's upper atmosphere; those produced through anthropogenic sources on the surface are broken down by solar radiation at much lower altitudes. However, hydrocarbons can be introduced into the upper atmosphere in situ in the vicinity of a space vehicle, for instance through surface outgassing or leakage of unburned fuel. For a vehicle in low-earth orbit with a velocity of 7.8 km s⁻¹, the resultant collisions with ambient atmospheric species take place with center-of-mass collision energies *E*_{COM} on the order of several hundred kJ mol⁻¹. For a suborbital vehicle with an apogee in the 100–150 km range, the interaction energies are much lower, in the 10–50 kJ mol⁻¹ range, though still significantly superthermal.

Above about 80-km altitude, ground-state O(³P) atoms become increasingly prevalent owing to solar VUV photodissociation of O₂. The O-atom density peaks at about 100 km, with concentrations exceeding 10¹¹ cm⁻³,¹ and exceeds the O₂ density for altitudes above about 120 km. The presence of O atoms is important in part because O is much more reactive than the other prevalent neutral constituents, N₂ and O₂. The high collision energies that are possible—for instance, 310 kJ mol⁻¹ for O–C₂H₄ collisions at the orbital velocity—serve to stimulate two phenomena: first, nonreactive excitation of the internal modes of the hydrocarbon, and second, chemical reaction by surmounting the potential barrier governing the reaction coordinate, resulting in various molecular and radical products. Lower energy processes, typically involving secondary chemistry, can also occur in the vehicle's wake, downstream of the initial interaction region near the ram surface. These

downstream radical–radical and molecule–radical reactions often occur at gas kinetic rates with little or no temperature dependence, giving rise to fast processes even in the relatively cool wake region. In both cases, the resultant physical excitation and chemical reaction processes yield rovibrationally excited products that often radiate in the infrared. The structure of this emission could provide a signature as to the type and/or origin of the vehicle in question.

In this report, we provide results from a recently initiated experiment detecting the products of C₂H₄–O collisions. The C₂H₄–O system was chosen for several reasons: (1) alkenes are common components of missile fuels, (2) the chemistry, even for the simplest alkene, is complex and results in a host of IR-active products, and (3) the study complements work being performed in our laboratory with laser-induced fluorescence detection of the product HCO radical.² Two long-term goals of this work are to determine detailed product state information and to observe the role of translational energy in the reactions. Reactions of alkenes with O atoms have undergone a large amount of study within both the combustion³ and chemical dynamics communities.^{4,5} Figure 1 shows a schematic of the principal reaction pathways available to O + C₂H₄ encounters. The main product channels are an H-atom–vinoxy radical pair (H + CH₂CHO) and a formyl–methyl radical pair (HCO + CH₃). There is some disagreement as to the partitioning between these channels,^{4,6–8} though each accounts for roughly half of the overall product yield. According to at least one study, the methylene–formaldehyde (CH₂ + CH₂O) channel accounts for a few percent of the yield.⁷ The further unimolecular dissociation of CH₂CHO to several different products has also been studied,^{6,9} as has that of HCO to H + CO, both experimentally^{10–12} and theoretically.^{13–16} The H–CO dissociation channel is shown with its approximately 96 kJ mol⁻¹ barrier, together with the lowest four product CO vibrational levels.

In this work, vibrationally excited products such as CO, CO₂, HCO, and H₂CO have been detected via emission, using the technique of time-resolved Fourier transform infrared (FTIR)

* Address correspondence to this author. E-mail: james.dodd@hanscom.af.mil.

[†] Current address: Stewart Radiance Laboratory, 139 The Great Road, Bedford, MA 01730.

[‡] Current address: Bucknell University, Department of Chemistry, Lewisburg, PA 17837.

[§] Current address: LeTourneau University, Department of Chemistry and Physics, Longview, TX 75607-7001.

REPORT DOCUMENTATION PAGE				Form Approved OMB No. 0704-01-0188		
<p>The public reporting burden for this collection of information is estimated to average 1 hour per response, including the time for reviewing instructions, searching existing data sources, gathering and maintaining the data needed, and completing and reviewing the collection of information. Send comments regarding this burden estimate or any other aspect of this collection of information, including suggestions for reducing the burden to Department of Defense, Washington Headquarters Services Directorate for Information Operations and Reports (0704-0188), 1215 Jefferson Davis Highway, Suite 1204, Arlington VA 22202-4302. Respondents should be aware that notwithstanding any other provision of law, no person shall be subject to any penalty for failing to comply with a collection of information if it does not display a currently valid OMB control number.</p> <p>PLEASE DO NOT RETURN YOUR FORM TO THE ABOVE ADDRESS.</p>						
1. REPORT DATE (DD-MM-YYYY) 11-20-2004		2. REPORT TYPE REPRINT		3. DATES COVERED (From - To)		
4. TITLE AND SUBTITLE O + C _n H _{2n} Products Detected via IR Emission. 1. O + C ₂ H ₄				5a. CONTRACT NUMBER		
				5b. GRANT NUMBER		
				5c. PROGRAM ELEMENT NUMBER 61102F		
6. AUTHORS James A. Dodd, Eunsook S. Hwang*, Karen J. Castle**, and Gary D. DeBoer [#]				5d. PROJECT NUMBER 2303		
				5e. TASK NUMBER HS		
				5f. WORK UNIT NUMBER A1		
7. PERFORMING ORGANIZATION NAME(S) AND ADDRESS(ES) Air Force Research Laboratory /VSBYH 29 Randolph Road Hanscom AFB, MA 01731-3010				8. PERFORMING ORGANIZATION REPORT NUMBER AFRL-VS-HA-TR-2006-1004		
9. SPONSORING/MONITORING AGENCY NAME(S) AND ADDRESS(ES)				10. SPONSOR/MONITOR'S ACRONYM(S) AFRL/VSBYH		
				11. SPONSOR/MONITOR'S REPORT NUMBER(S)		
12. DISTRIBUTION/AVAILABILITY STATEMENT Approved for public release; distribution unlimited.						
13. SUPPLEMENTARY NOTES REPRINTED FROM: J. Phys. Chem A, 2004, Vol. 108, pp. 10965-10972 © 2004, American Chemical Society. *Stewart Radiance Lab., Bedford, MA 01730. **Bucknell Univ., Dept. of Chemistry, Lewisburg, PA 17837. #LeTourneau Univ., Longview, TX 75607-7001						
14. ABSTRACT, Collisions between oxygen atoms and ethene have been investigated by using infrared emission detection of the chemiluminescent product species. A prototypical alkene, ethene, nonetheless exhibits numerous reaction pathways in reactions with O atoms. Oxygen atoms were formed via photolysis of SO ₂ in the presence of C ₂ H ₄ , and the resultant IR emissions in the 900-3000 cm ⁻¹ spectral region were detected by using a time-resolved, step-scan Fourier transform spectrometer. A Welsh cell mirror arrangement was used to maximize the collection efficiency of the product IR emissions. Vibrationally excited products such as CO, CO ₂ , HCO, and H ₂ CO have been identified, with CO and CO ₂ being the dominant IR emitters. The time-evolving CO and CO ₂ spectra have been characterized with respect to the SO ₂ and C ₂ H ₄ partial pressures and laser fluence. The rate constants for vibrational relaxation of CO ₂ high-v population by C _n H _{2n} (n=2-4) are in the mid 10 ⁻¹² cm ³ s ⁻¹ range; SO ₂ is a very inefficient relaxer. A chemical kinetics code has been used to model the chemistry and identify the operative reaction mechanisms, including the effects of secondary chemistry.						
15. SUBJECT TERMS Infrared emission Chemiluminescence Hydrocarbon chemistry Atomic oxygen Fourier transform spectroscopy Vibrational excitation						
16. SECURITY CLASSIFICATION OF:			17. LIMITATION OF ABSTRACT	18. NUMBER OF PAGES	19a. NAME OF RESPONSIBLE PERSON Steven Lipson	
a. REPORT UNCL	b. ABSTRACT UNCL	c. THIS PAGE UNCL	UNL	9	19b. TELEPHONE NUMBER (Include area code) (781) 377-3626	

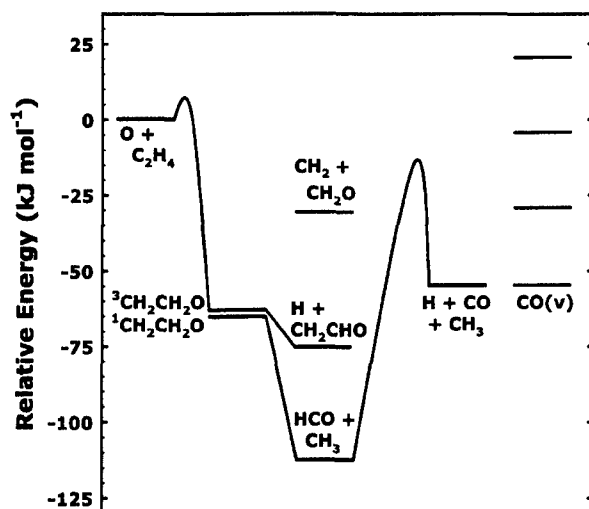


Figure 1. Reaction path schematic of the $\text{O} + \text{C}_2\text{H}_4$ reaction, including the 6.65 kJ mol^{-1} room temperature activation barrier (ref 27). The principal direct reaction channels are $\text{H} + \text{CH}_2\text{CHO}$ and $\text{HCO} + \text{CH}_3$, where each represents about half of the overall product yield. The $\text{H}_2 + \text{CH}_2\text{O}$ channel accounts for a few percent of the yield (ref 7). The $\text{H}-\text{CO}$ dissociation channel is shown with its approximately 96 kJ mol^{-1} barrier, as well as the lowest four CO vibrational level energies.

spectroscopy. While FTIR emission detection is a versatile and powerful means of observing the IR-active products in a reaction mixture, it has the disadvantage of low sensitivity relative to other detection methods. Thus, the species partial pressures are necessarily relatively high to ensure adequate signal-to-noise ratios for detection purposes. Under these conditions, secondary chemistry plays a significant role in the production of IR-active species. To better understand the chemistry occurring in the reaction cell following the excitation pulse, a chemical kinetics model was employed to predict species concentrations as a function of time after laser excitation, including the effects of secondary chemistry following the initial $\text{O} + \text{C}_2\text{H}_4$ reaction.

2. Experimental Section

Oxygen atoms were generated through the 193-nm photolysis of SO_2 with use of 95-mJ light pulses from a 30-Hz Lambda-Physik Lextra 200 excimer laser. The SO_2 photolysis produces a relatively peaked distribution of O-atom energies, centered at 27.0 kJ mol^{-1} laboratory frame energy,^{17–20} or 17.2 kJ mol^{-1} COM energy for the $\text{O}-\text{C}_2\text{H}_4$ interaction. Mass flows of 15 standard atm $\text{cm}^3 \text{ min}^{-1}$ (sccm) SO_2 , 15 sccm C_2H_4 , and 100 sccm Ar bath gas were passed through a reaction cell at a total pressure of 500 mTorr. The cell was fitted with UV-fused silica windows for the laser excitation pulses and a CaF_2 window, positioned at 90° , for sampling the IR chemiluminescence. The gas mix was introduced and evacuated via opposing 2.54-cm-diameter pipes separated by 10 cm. The cell contained a pair of 10.2-cm-diameter, 10.2-cm radius-of-curvature aluminum-coated mirrors arranged in the Welch cell configuration^{21–24} for collection of IR chemiluminescent emission. A portion of the Ar bath gas was used to purge the sidearms supporting the laser windows and the mirrors.

The IR emission exiting the cell reflected off two aluminum mirrors into a Bruker IFS/66 step-scan spectrometer, capable of obtaining simultaneous spectrally and temporally resolved data. For these experiments the nominal spectral resolution was either 2 or 15 cm^{-1} , with 250 time samples of 5- μs time resolution collected following laser excitation. Emission data from up to 100 laser shots, or 3.3-s real time at the 30-Hz

TABLE 1: IR Emissions in the 1000–3500 cm^{-1} Spectral Range, from 193-nm Laser Excitation of Sample Gas Mixtures

gas(es) present ^a	principal IR emissions, cm^{-1}	emitting bands
$n\text{-C}_4\text{H}_8$	2750–3350	aliphatic C–H stretch modes
SO_2	1150, 1360	$\text{SO}(\nu)$, $\text{SO}_2(\nu_1, \nu_3)$
$\text{SO}_2 + \text{CO}$	1150, 1360	$\text{SO}(\nu)$, $\text{SO}_2(\nu_1, \nu_3)$
$\text{SO}_2 + n\text{-C}_4\text{H}_8$	1150, 1360	$\text{SO}(\nu)$, $\text{SO}_2(\nu_1, \nu_3)$
	1900–2300	$\text{CO}(\nu)$, $\text{CO}_2(\nu_3)$
	2400–3000	$\text{HCO}(\nu_1)$, $\text{H}_2\text{CO}(\nu_1, \nu_5)$

^a In addition to Ar bath gas.

repetition rate, were averaged at each mirror position. A 1-mm square HgCdTe detector was employed as either “openband” to cover the 900–3500 cm^{-1} range or with a cold band-pass filter limiting transmission to the 1950–2550 cm^{-1} range (“filter” data). The real time required to obtain a data matrix of two-dimensional information is proportional to the wavenumber band-pass divided by the spectral resolution. Thus, acquiring a filter data matrix could be accomplished in about one-quarter the time required for an openband data matrix with equivalent S/N.

With the 3.3 L s^{-1} pumping speed, the e -fold pumpdown time in the 5.6-L-volume reaction cell is equal to several seconds. However, the volume in the cylinder between the input and output pipes, 50 mL, is evacuated on a time scale of tens of milliseconds. Since the reactant gases are introduced wholly through the input pipe, while the Ar bath gas is introduced mainly through the sidearms and more remote portions of the cell, the latter time scale is likely to be a more accurate measure of the residence time of the reactive gas mixture. A buildup of certain reaction products could complicate the chemistry, for instance through the photolysis of CH_2O . To test whether this was affecting the present results, the experiment was run at 10 Hz in addition to the normal 30 Hz; the slower repetition rate significantly decreases any buildup of reaction products between laser pulses. Decreasing the repetition rate caused no discernible effect in the observed time-dependent IR spectra for the gas flows used herein.

Table 1 summarizes a series of control experiments to check for the source of the emissions ascribed to chemical reaction between O and C_2H_4 . All the species were dilute in Ar bath gas in a roughly 1:1 ratio when more than one minor species was present. The alkene n -but-1-ene ($n\text{-C}_4\text{H}_8$) used for these experiments has a much larger 193-nm absorption coefficient than C_2H_4 , with the absorption cross section $\sigma_{193}(n\text{-C}_4\text{H}_8) = 5.9 \times 10^{-19} \text{ cm}^2$ ²⁵ equal to about 5% of $\sigma_{193}(\text{SO}_2) = 1.2 \times 10^{-17} \text{ cm}^2$. Thus, the photolysis of neat $n\text{-C}_4\text{H}_8$ provides a stringent test regarding the possible formation of chemiluminescent hydrocarbon fragmentation and/or reaction products. As seen in Table 1, 193-nm photolysis of dilute $n\text{-C}_4\text{H}_8$ produced only short-lived emission ($<40 \mu\text{s}$) in the 2750–3350 cm^{-1} region, corresponding to aliphatic C–H stretch emission at higher wavenumber values than those relevant to the analysis below. Photolysis of neat SO_2 or SO_2 – CO mixtures gave rise to SO_2 photoproducts only. Finally, photolysis of SO_2 – $n\text{-C}_4\text{H}_8$ mixtures produced the CO and CO_2 emissions in the 1900–2300 cm^{-1} region analyzed herein.

3. Results and Discussion

3.1. IR Radiance Observations. Figure 2 provides a three-dimensional “waterfall” view of openband emission spectra at selected time delays following laser excitation of the SO_2 – C_2H_4 –Ar gas mixture. Various IR bands are observed, consis-

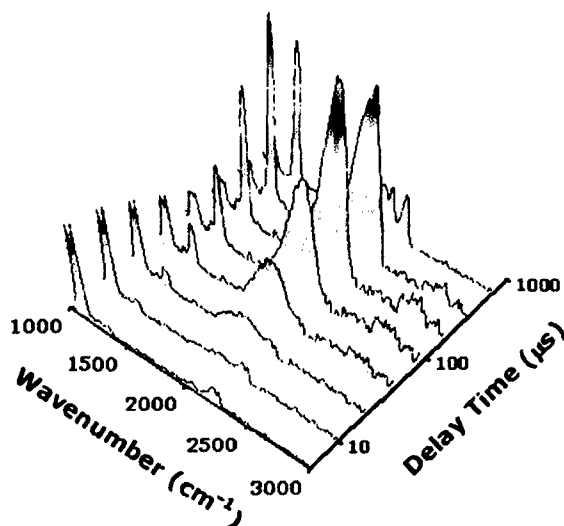


Figure 2. Time evolution of openband IR emission spectra resulting from 193-nm laser excitation of an SO₂-C₂H₄-Ar gas mixture, in the 1000–3000 cm⁻¹ wavenumber region with 15-cm⁻¹ resolution. Sample spectra are shown for the 5–640 μs delay time range on a log scale, with each successive spectrum delayed an additional factor of 2 in time. The spectra have been corrected for detector response. See text for description of features.

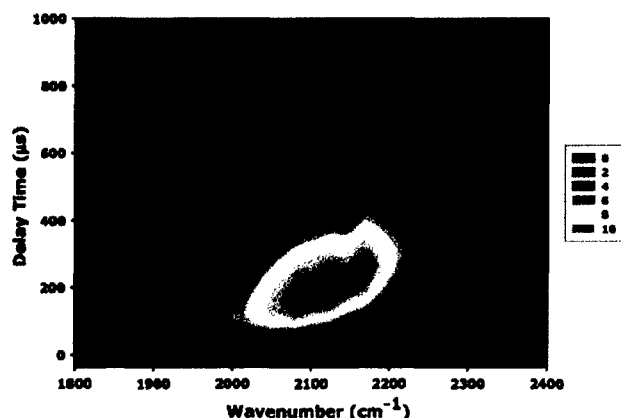


Figure 3. Time evolution of openband IR emission spectra resulting from 193-nm laser excitation of an SO₂-C₂H₄-Ar gas mixture, in the 1800–2400 cm⁻¹ wavenumber region with 15-cm⁻¹ resolution. Fundamental, hot band, and combination ν₃ emission are observed from vibrationally excited CO₂, together with overlying fundamental and hot band CO (ν → ν - 1) emission. The CO₂ emission is partially absorbed by about 1 m of room air, especially for wavenumber values larger than 2300 cm⁻¹. The data have been corrected for detector response.

tent with emission from the chemiluminescent CO (ν → ν - 1) and CO₂ ν₃ (1900–2300 cm⁻¹), H-CO ν₁ (2438 cm⁻¹), and H₂CO ν₁ and ν₅ (2450–3000 cm⁻¹) modes, as well as from the precursor species SO₂ ν₁ (1151 cm⁻¹) and ν₃ (1362 cm⁻¹) and SO (ν → ν - 1) (1150 cm⁻¹) modes, the last of which is overlapped with SO₂ ν₁. There is also evidence of parent C₂H₄ ν₇ (949 cm⁻¹) and ν₁₂ (1444 cm⁻¹) emission. A disadvantage of the FTIR detection technique, at least at low resolution, is that intense emissions can obscure others that are not as intense. For example, the very strong CO and CO₂ features could be concealing weak HCO ν₂ emission at 1868 cm⁻¹.

Figure 3 shows details of the spectral region dominated by CO₂ (ν₃ → ν₃ - 1) asymmetric stretch and CO (ν → ν - 1) fundamental emissions, using a color-coded contour plot representation of the openband spectrum. Emission from highly vibrationally excited CO₂ and, to a lesser extent, CO results in

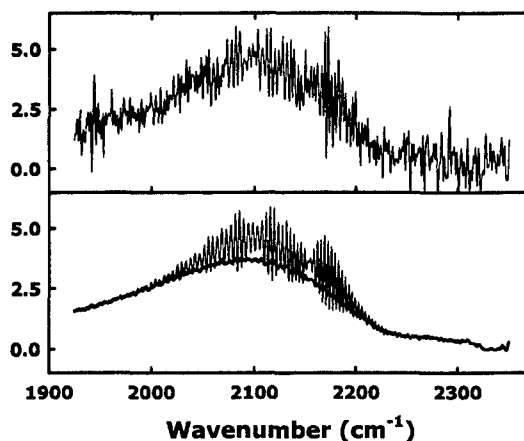


Figure 4. Top: Emission spectrum resulting from 193-nm laser excitation of an SO₂-C₂H₄-Ar gas mixture, in the 1925–2350 cm⁻¹ wavenumber region with 2-cm⁻¹ resolution. The spectrum was obtained 100 μs after the laser pulse. Bottom: Synthetic spectral fit consisting of sharp CO lines superimposed on a broad CO₂ emission feature. The bold line highlights the CO₂ contribution. See text for discussion.

hot and combination bands that shift the radiance to lower wavenumber values. The CO ν populations are collisionally relaxed relatively slowly, as evidenced by the “fingers” at 2100 and 2175 cm⁻¹ extending to long delay times. These are the P and R branches of the ν = 1 → 0 fundamental band, which is the last band to be relaxed as the vibrational populations cascade downward. Preliminary synthetic spectral modeling of the CO ν emissions is consistent with a Boltzmann-weighted vibrational distribution, with an effective vibrational temperature of about 4000 K at small delay times.²⁶

For the CO₂ emission profile, preliminary modeling is also consistent with a highly excited vibrational distribution closely following the excitation laser pulse.²⁶ At early times the emitting populations have undergone negligible vibrational relaxation, and the radiance in a spectral region that preferentially samples CO₂ can be taken as proportional to the CO₂ production rate. For the most highly vibrationally excited CO₂ populations, corresponding to those radiating in the longest wavelength portion of the spectrum, there is negligible feed from higher lying populations. This lack of feed simplifies the vibrational relaxation measurements discussed below. The 1900–2000 cm⁻¹ spectral region is convenient in monitoring the CO₂ population evolution: the emission is strong enough to easily detect, it is occurring from high-lying vibrational levels of CO₂, and radiance from CO₂ dominates, especially at early times. Spectral fitting indicates that in the 1900–2000 cm⁻¹ region, the CO ν radiance contributes at most a few percent over the first 400 μs. At later times the contribution by radiating CO ν increases, but the overall intensity becomes very small and the decay has negligible effect on the results of the CO₂ population kinetic analysis. Figure 4 shows a sample synthetic spectral fit to a 100-μs delay spectrum for an excited SO₂-C₂H₄-Ar gas mixture. The model spectrum consists of predicted emission from CO vibrational populations characterized by a 2500 K effective temperature, and from a distribution of CO₂ rovibrational populations with energies up to 40 000 cm⁻¹. As is evident, virtually all of the radiance for wavenumber values <2000 cm⁻¹ is due to emission from excited CO₂.

3.2. O-Atom Thermalization and Chemistry. The COM energy of the O + C₂H₄ system afforded by photolysis of SO₂ is equal to 17.2 kJ mol⁻¹, which is sufficient to overcome the 6.65 kJ mol⁻¹ room temperature activation barrier (Figure 1).²⁷ The O-C₂H₄ reaction rate constant is strongly temperature

TABLE 2: Rate Constants Employed in the Chemical Kinetics Model, in Units of $\text{cm}^3 \text{s}^{-1}$

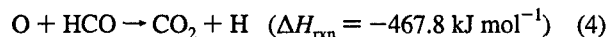
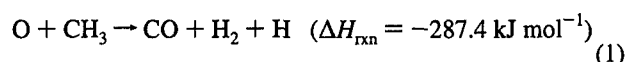
$\text{C}_2\text{H}_4 + \text{O} \rightarrow \text{CH}_2\text{CHO} + \text{H}$	3.75×10^{-13}	$\text{CH}_3 + \text{CH}_3\text{CO} \rightarrow \text{CH}_3\text{COCH}_3$	7.01×10^{-11}
$\text{C}_2\text{H}_4 + \text{O} \rightarrow \text{CH}_3 + \text{HCO}$	3.30×10^{-13}	$\text{CH}_3 + \text{CH}_3\text{CO} \rightarrow \text{CH}_4 + \text{CH}_2\text{CO}$	1.01×10^{-11}
$\text{C}_2\text{H}_4 + \text{O} \rightarrow \text{CH}_2\text{CO} + \text{H}_2$	7.50×10^{-15}	$\text{CH}_3 + \text{CH}_2\text{CO} \rightarrow \text{CO} + \text{C}_2\text{H}_3$	8.30×10^{-12}
$\text{C}_2\text{H}_4 + \text{O} \rightarrow \text{CH}_2 + \text{CH}_2\text{O}$	4.50×10^{-14}	$\text{CH}_2\text{CO} + \text{CH}_2 \rightarrow \text{CH}_3 + \text{HCO}$	1.00×10^{-14}
$\text{C}_2\text{H}_4 + \text{O} \rightarrow \text{C}_2\text{H}_3 + \text{OH}$	2.56×10^{-15}	$\text{CH}_3\text{CO} + \text{H} \rightarrow \text{CH}_3 + \text{HCO}$	3.56×10^{-11}
$\text{CH}_2\text{O} + \text{O} \rightarrow \text{HCO} + \text{OH}$	1.73×10^{-13}	$\text{CH}_3\text{CO} + \text{H} \rightarrow \text{CH}_2\text{CO} + \text{H}_2$	1.92×10^{-11}
$\text{CH}_2\text{O} + \text{OH} \rightarrow \text{HCO} + \text{H}_2\text{O}$	1.00×10^{-11}	$\text{CH}_3\text{CO} + \text{OH} \rightarrow \text{CH}_2\text{CO} + \text{H}_2\text{O}$	2.01×10^{-11}
$\text{CH}_3\text{CO} + \text{O} \rightarrow \text{CH}_2\text{CO} + \text{OH}$	6.40×10^{-11}	$\text{CH}_3\text{CO} + \text{O}_2 \rightarrow \text{CH}_3\text{O} + \text{CO}_2$	4.51×10^{-13}
$\text{CH}_3\text{CO} + \text{O} \rightarrow \text{CO} + \text{CH}_3$	2.56×10^{-10}	$\text{CH}_2\text{CO} + \text{H} \rightarrow \text{CO} + \text{CH}_3$	7.32×10^{-13}
$\text{CH}_3\text{CO} + \text{CH}_2 \rightarrow \text{CH}_2\text{CO} + \text{CH}_3$	3.01×10^{-11}	$\text{HCO} + \text{H} \rightarrow \text{CO} + \text{H}_2$	1.13×10^{-10}
$\text{CH}_2 + \text{O} \rightarrow \text{HCO} + \text{H}$	5.01×10^{-11}	$\text{HCO} + \text{OH} \rightarrow \text{CO} + \text{H}_2\text{O}$	1.69×10^{-10}
$\text{CH}_2 + \text{O} \rightarrow \text{CO} + \text{H}_2$	8.00×10^{-11}	$\text{HCO} + \text{CH}_2 \rightarrow \text{CO} + \text{CH}_3$	3.01×10^{-11}
$\text{CH}_2 + \text{O} \rightarrow \text{CO} + 2\text{H}$	1.20×10^{-10}	$\text{HCO} + \text{CH}_3\text{CO} \rightarrow \text{CH}_3\text{COCHO}$	3.01×10^{-11}
$\text{CH}_2 + \text{O} \rightarrow \text{CH} + \text{OH}$	7.20×10^{-12}	$\text{HCO} + \text{HCO} \rightarrow \text{CH}_2\text{O} + \text{CO}$	5.00×10^{-11}
$\text{CH}_3 + \text{O} \rightarrow \text{CH}_2\text{O} + \text{H}$	9.50×10^{-11}	$\text{HCO} + \text{O}_2 \rightarrow \text{CO} + \text{HO}_2$	3.86×10^{-12}
$\text{CH}_3 + \text{O} \rightarrow \text{CO} + \text{H}_2 + \text{H}$	4.00×10^{-11}	$\text{HCO} + \text{CO} \rightarrow 2\text{CO} + \text{H}_2$	3.64×10^{-11}
$\text{CH}_3 + \text{O} \rightarrow \text{CH}_3\text{O}$	2.60×10^{-14}	$\text{HCO} + \text{HCO} \rightarrow \text{CHOCHO}$	5.00×10^{-11}
$\text{HCO} + \text{O} \rightarrow \text{CO} + \text{OH}$	5.00×10^{-11}	$\text{CH}_3\text{O} + \text{CH}_3\text{CO} \rightarrow \text{CH}_2\text{O} + \text{CH}_3\text{CHO}$	1.00×10^{-11}
$\text{CH}_3\text{CHO} + \text{O} \rightarrow \text{CH}_3\text{CO} + \text{OH}$	3.90×10^{-13}	$\text{CH}_3\text{O} + \text{CH}_3\text{CO} \rightarrow \text{CH}_3\text{OH} + \text{CH}_2\text{CO}$	1.00×10^{-11}
$\text{HCO} + \text{O} \rightarrow \text{CO}_2 + \text{H}$	5.00×10^{-11}	$\text{CH}_2\text{OCH}_2 \rightarrow \text{CH}_3 + \text{HCO}$	1.00×10^{-14}
$\text{OH} + \text{O} \rightarrow \text{O}_2 + \text{H}$	2.50×10^{-11}	$\text{CH}_3\text{CHO} + \text{CH}_3\text{CO} \rightarrow (\text{CH}_3)_2\text{CO} + \text{HCO}$	2.84×10^{-13}
$\text{OH} + \text{CO} \rightarrow \text{CO}_2 + \text{H}$	1.26×10^{-13}	$\text{CH}_3\text{O} + \text{HCO} \rightarrow \text{CH}_3\text{OH} + \text{CO}$	1.50×10^{-10}
$\text{CH}_2\text{CO} + \text{CH}_2 \rightarrow \text{C}_2\text{H}_4 + \text{CO}$	2.09×10^{-10}	$\text{H} + \text{HCCO} \rightarrow \text{CO} + \text{CH}_2$	2.49×10^{-10}
$\text{CH}_3 + \text{OH} \rightarrow \text{H}_2 + \text{HOCH}$	6.13×10^{-13}	$\text{H} + \text{CH}_2 \rightarrow \text{H}_2 + \text{CH}$	4.92×10^{-10}
$\text{CH}_3 + \text{OH} \rightarrow \text{CH}_2\text{OH} + \text{H}$	1.31×10^{-11}	$\text{CH}_3 + \text{CH}_2\text{OH} \rightarrow \text{CH}_2\text{O} + \text{CH}_4$	1.41×10^{-10}
$\text{CH}_3 + \text{OH} \rightarrow \text{CH}_3\text{OH}$	1.69×10^{-10}	$\text{CH}_3 + \text{SO}_2 \rightarrow \text{CH}_3\text{SO}_2$	2.91×10^{-13}
$\text{CH}_3 + \text{OH} \rightarrow \text{H}_2\text{O} + \text{CH}_2$	1.13×10^{-12}	$\text{SO} + \text{OH} \rightarrow \text{SO}_2 + \text{H}$	8.60×10^{-11}
$\text{CH}_3 + \text{CH}_2 \rightarrow \text{C}_2\text{H}_4 + \text{H}$	7.01×10^{-11}	$\text{CH}_2\text{CO} + \text{OH} \rightarrow \text{CH}_2\text{O} + \text{HCO}$	4.65×10^{-11}
$\text{CH}_3 + \text{CH}_2\text{OH} \rightarrow \text{C}_2\text{H}_5\text{OH}$	2.01×10^{-11}	$\text{O}_2 + \text{SO} \rightarrow \text{SO}_2 + \text{O}$	8.65×10^{-17}
$\text{CH}_3 + \text{CH}_3\text{CO} \rightarrow \text{C}_2\text{H}_6 + \text{CO}$	5.40×10^{-11}	$\text{CH}_2\text{CO} + \text{OH} \rightarrow \text{H}_2\text{O} + \text{HCCO}$	1.19×10^{-13}
$\text{CH}_3 + \text{HCO} \rightarrow \text{CH}_3\text{CHO}$	3.01×10^{-11}	$\text{CH}_2\text{CO} + \text{OH} \rightarrow \text{CH}_2\text{OH} + \text{CO}$	7.10×10^{-12}
$\text{CH}_3 + \text{HCO} \rightarrow \text{CH}_4 + \text{CO}$	4.40×10^{-11}		

dependent,²⁸ with a room temperature reaction rate of $7.5 \times 10^{-13} \text{ cm}^3 \text{s}^{-1}$. Prior to any collisional relaxation of the nascent O atoms, the O–C₂H₄ interaction energy corresponds to a kinetic temperature of about 2000 K, for which the reaction rate constant is 45 times higher, or $3.4 \times 10^{-11} \text{ cm}^3 \text{s}^{-1}$. A small portion of the reaction products occurs through collisions involving fast O atoms. Ethene is present in a 0.11 mol fraction in the gas mixture and thus about 1% of the initially formed fast O reacts prior to thermalization. It can be seen from Figure 2 that aside from prompt emission from SO ν and/or SO₂ ν_1 near 1150 cm^{-1} , the majority of the emission has a delayed appearance, consistent with primary chemistry induced by thermalized O atoms and/or secondary chemistry. The rate of thermalization of the energetic O atoms can be estimated by using the data of Matsumi et al.,²⁹ who found that 41-kJ mol⁻¹ O(¹D) atoms are translationally thermalized by Ar with a near-gas kinetic rate constant of $1.28 \times 10^{-10} \text{ cm}^3 \text{s}^{-1}$. Assuming O(³P) is thermalized by Ar with a similar efficiency, and that Ar is representative of the gas mixture in general, at 0.5-Torr pressure the e -fold time for thermalization is about 0.5 μs . Thus the IR emissions from the chemical reaction products discussed herein arise principally from thermal chemistry.

The reactions of O atoms with small-chain alkenes have been studied extensively in recent years by Bersohn and co-workers.^{9,30–33} The mechanism involves addition of O(³P) to the alkene double bond to form a triplet biradical. The biradical can either dissociate directly to produce vinoxy radical and an H atom or intersystem cross to the singlet state. In the singlet state the barrier to H-atom transfer is lowered dramatically, and the energized intermediate can give rise, through a combination of H-atom migration and dissociation, to a host of daughter species.

According to the literature, CO and CO₂ are not nascent products of the O + C₂H₄ reaction. However, both of these species can be formed through highly exothermic secondary reactions, with ΔH_{rxn} values in the –290 to –470 kJ mol⁻¹

range. The principal formation processes as identified by the kinetic model described below are given by



These energy releases are sufficient to populate highly excited vibrational levels of the product CO and CO₂ even in the absence of translationally excited reactants. The details of the CO and CO₂ vibrational population distributions and formation mechanisms will be discussed in a forthcoming publication.²⁶

3.3. Modeling of Chemistry. To identify the chemical formation mechanisms of the principal IR-emitting products, including CO and CO₂, a chemical kinetics model was developed that employs the commercial REACT computer code.³⁴ Given initial concentrations and standard chemical kinetic inputs, the model integrates the coupled differential equations describing the set of chemical reactions and predicts the species concentrations as a function of time, with an integration step size of 5 μs . All reactions were characterized by their 295 K rate constants. A total of 40 species and 65 reactions were included in the model with the parameters obtained from multiple sources, notably from the review of Baulch et al.²⁸ Table 2 details the chemical reactions and associated rate constants used in the model.

Figure 5 shows the predicted time-dependent species concentrations for the gas mixture described in the Experimental Section, assuming SO₂ photolysis takes place at $t = 0$, initiating the chemistry. About a third of the SO₂ is dissociated by the typical laser fluence used. The model can easily predict the

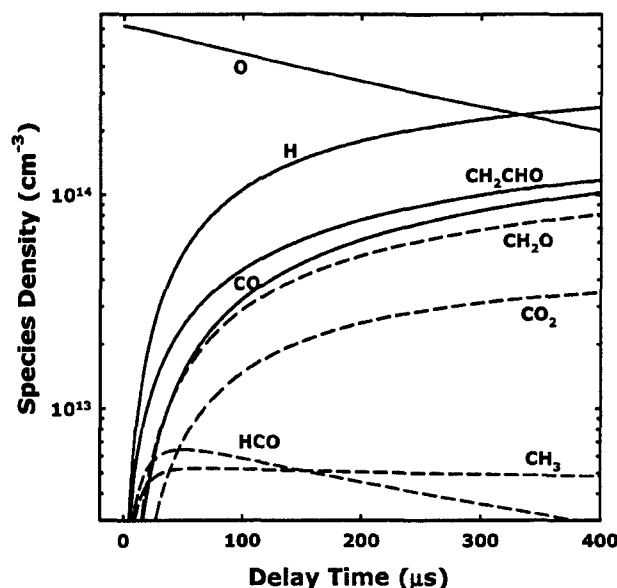
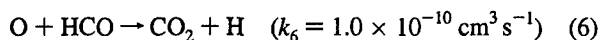
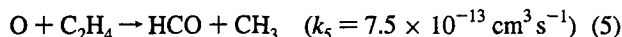


Figure 5. Species concentrations predicted by the chemical kinetics model. The reaction chemistry is initiated at time $t = 0$ through the 193-nm photolysis of $1.9 \times 10^{15} \text{ cm}^{-3}$ of SO₂ to produce SO + O(³P), with the O atoms reacting with $1.9 \times 10^{15} \text{ cm}^{-3}$ C₂H₄ to produce numerous products. Approximately 40 chemical species and 65 separate reactions were included in the model. Reaction rates and product branching ratios were taken principally from ref 28. The model assumes thermal chemistry throughout.

product species formation rates as a function of the inputted initial O and ethene concentrations. These predictions are compared with the experimental observations in the discussion below. In this study we focus on CO₂ production, probed by emission from highly excited vibrational levels in the 1900–2000 cm^{−1} spectral region.

3.3.1. Dependence of CO₂ Emission Intensity on [O]_{initial}. The band intensity for excited CO₂, integrated between 1900 and 2000 cm^{−1} and 0–50 μs, is shown as a function of O-atom concentration on a log–log scale in Figure 6a for the density range appropriate for the experiment. Two experimentally determined curves are shown, varying the laser fluence and the SO₂ concentration, since both serve to increase the initial O-atom concentration. The integrated radiance reaches a maximum at a delay time that is independent of fluence or SO₂ concentration, and thus the time integration is a good representation of the rate of formation of vibrationally excited CO₂ product. The slope for the log–log plot provides an estimate for the order of the process that gives rise to the IR-emitting CO₂. In Figure 6b, the model prediction for CO₂ chemical production as a function of the initial O-atom density is shown. The average slope predicted by the chemical model, 1.42, falls midway between the experimental values of 1.31 and 1.61, confirming that the dependence is intermediate between linear and quadratic. The cause of the discrepancy between the experimental laser fluence and SO₂ concentration results is not clear, though the slopes marginally agree to within the error bar limits.

The formation of CO₂ is dominated by the following two-step mechanism, shown with the room temperature rate constants:



Note that the energy released by reaction 6, $\Delta H_{\text{rxn}} = -467.8 \text{ kJ mol}^{-1}$, is sufficient to populate the highly excited CO₂

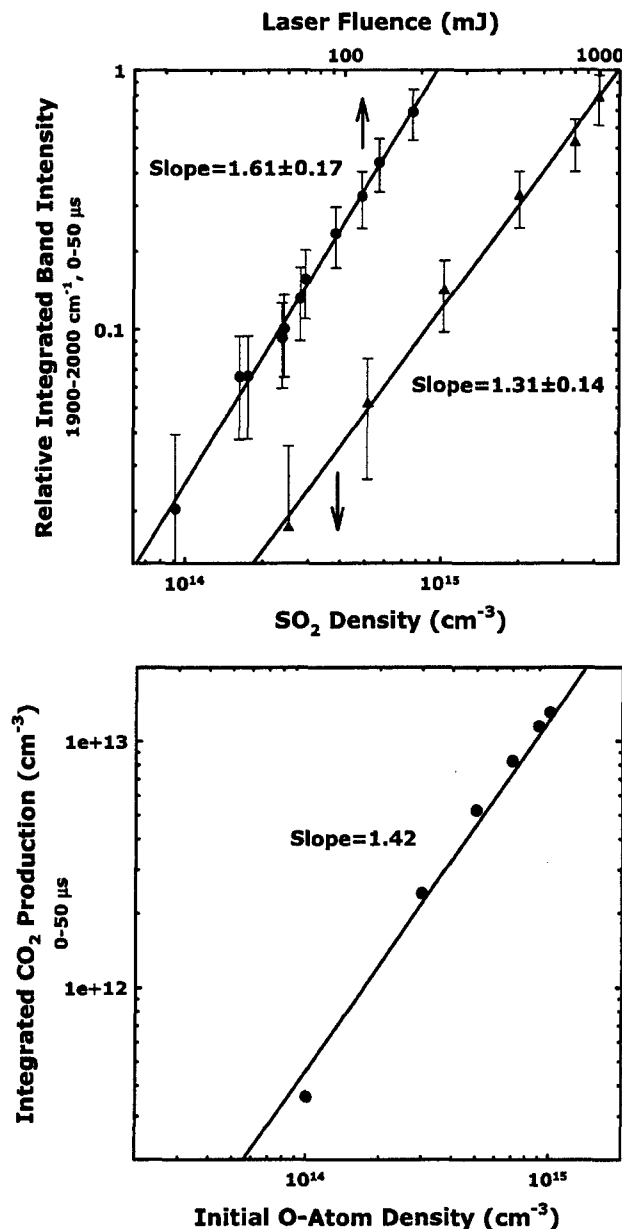


Figure 6. (a) Log–log plot of integrated band intensity of the CO₂ ν₃ emission region (1900–2000 cm^{−1}, 0–50 μs) vs the laser fluence (upper curve) and SO₂ density (lower curve). (b) Log–log plot of the chemical model prediction of integrated CO₂ production (0–50 μs) vs the initial O-atom density.

vibrational states observed in the data. For low initial O-atom concentrations the CO₂ chemical production rate is proportional to [O]² through the two-step process (5)–(6). For higher O-atom concentrations, the net HCO production rate falls to zero at short times following the photolysis pulse due to loss via reaction 6 and other processes; see Figure 5 for the predicted [HCO] time dependence for [O]_{initial} = $6 \times 10^{14} \text{ cm}^{-3}$. In the latter case the CO₂ production rate is linear, assuming the HCO concentration is approximately constant over the time integration period (0–50 μs). The chemical model reproduces this crossover from quadratic to linear behavior in [O].

3.3.2. Dependence of CO₂ Emission Intensity on [C₂H₄]. Figure 7a shows the CO₂ emission intensity, integrated between 1900 and 2000 cm^{−1} and 0–25 μs, plotted as a function of the C₂H₄ concentration; Figure 7b shows the predicted CO₂ chemi-

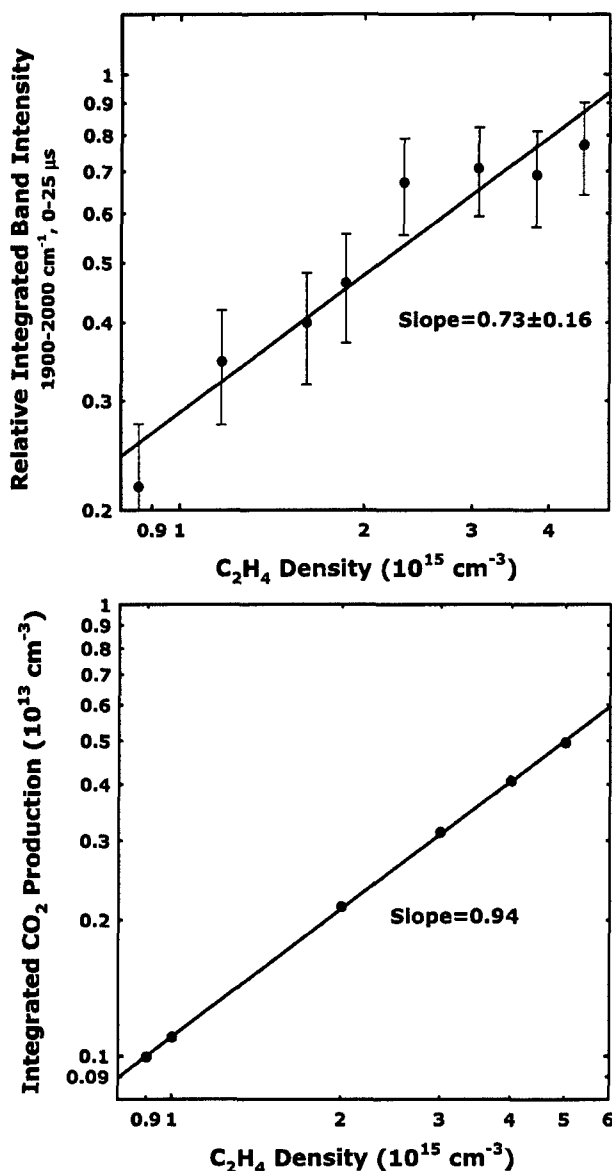


Figure 7. (a) Log-log plot of the integrated band intensity in the CO₂ ν_3 emission region (1900–2000 cm⁻¹, 0–25 μs) vs the C₂H₄ density. (b) Log-log plot of the chemical model prediction of integrated CO₂ production (0–25 μs) vs the C₂H₄ density.

cal production over the same time period. The C₂H₄ concentration range in Figure 7 is about 1–10 times that of [O]_{initial}. In this case the dependence should be approximately linear, since the CO₂ production rate is proportional to [C₂H₄] at early times according to the mechanism given by reactions 5–6. The average slope for the model prediction (0.94) is consistent with this, while the slope for the data is marginally lower, at 0.73 ± 0.16. The smaller value for the slope in Figure 7a could be due to differential quenching of the CO₂ emission by C₂H₄, even during the 0–25 μs time integration. This effect is discussed in the following section.

3.4. Vibrational Relaxation of CO₂ by C_nH_{2n}. For variable amounts of C₂H₄, the integrated radiance in the 1900–2000 cm⁻¹ region reaches a maximum at delay times that vary strongly as a function of the C₂H₄ concentration, indicating that C₂H₄ is an efficient relaxer of the vibrationally excited CO₂. Figure 8 shows the signal time evolution for three different C₂H₄ concentrations, showing how the maximum depends on the C₂H₄

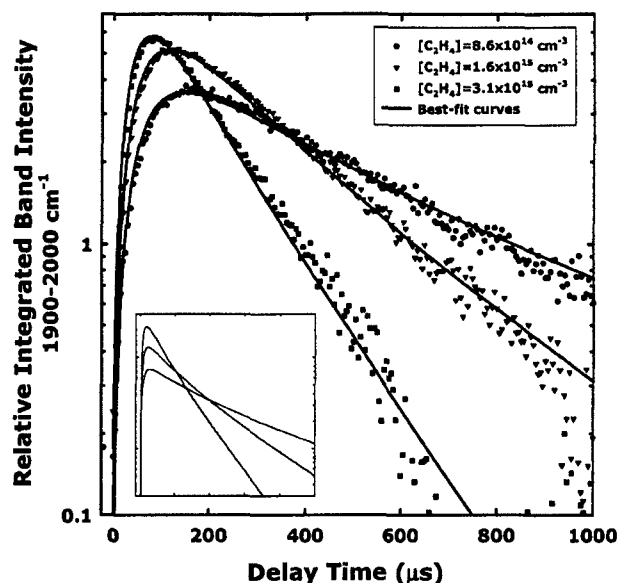


Figure 8. Semilog plot of the CO₂ ν_3 integrated emission (1900–2000 cm⁻¹) vs delay time, for three different C₂H₄ concentrations. The data were fit to eq 7 by varying the quenching rate Q and the scaling factor C . The inset shows the model CO₂ production rate $P(t)$ for the three C₂H₄ concentrations, on the same time and relative intensity scales as the data.

concentration. To estimate the decay rates, each curve was fit by integrating the expression

$$\frac{dI(t)}{dt} = CP(t) - QI(t) \quad (7)$$

In eq 7, $I(t)$ is the time-dependent signal intensity, $P(t)$ is the chemical production rate from the chemical kinetics model (in cm⁻³s⁻¹), Q is the relaxation rate (in s⁻¹), and C is an arbitrary constant relating the radiant intensity to the number density. Note that the quenching of the fluorescence only affects the rising portion and the magnitude of the population curves. The long-term decay rates are dictated by the decay of the feed term $P(t)$ as the O atoms are consumed by the rate-determining reaction 5. The decay of the feed term is well-matched by the kinetic model with no adjustable parameters, as shown in the inset to Figure 8.

The exponential decay constants for the relaxation of highly vibrationally excited CO₂ as a function of ethene, propene, and *n*-butene concentration are shown in Figure 9. The decay constants were obtained by fitting the 1900–2000 cm⁻¹ integrated emission time profile to eq 7 and plotting the best-fit disappearance rates Q against the alkene concentration. The feed functions $P(t)$ for propene and *n*-butene were assumed to be similar to that for ethene, with an approximately factor-of-five shorter time scale due to their faster reactions with O atoms.²⁷ Propene and *n*-butene were found to give rise to similar IR spectral profiles in reactions with O atoms; those results will be detailed in a future publication. As discussed above, the 1900–2000 cm⁻¹ spectral region contains emissions from highly excited CO₂ in a regime where cascade from higher levels is unlikely to present a major effect. For higher wavenumber bandpasses, the emission occurs from lower vibrational levels of CO₂ that are more prone to feed from higher levels. In particular, nonexponential decays at long times were observed when integrating over higher wavenumber ranges, consistent with a more complex feed mechanism and possibly a contribution from radiating CO ν .

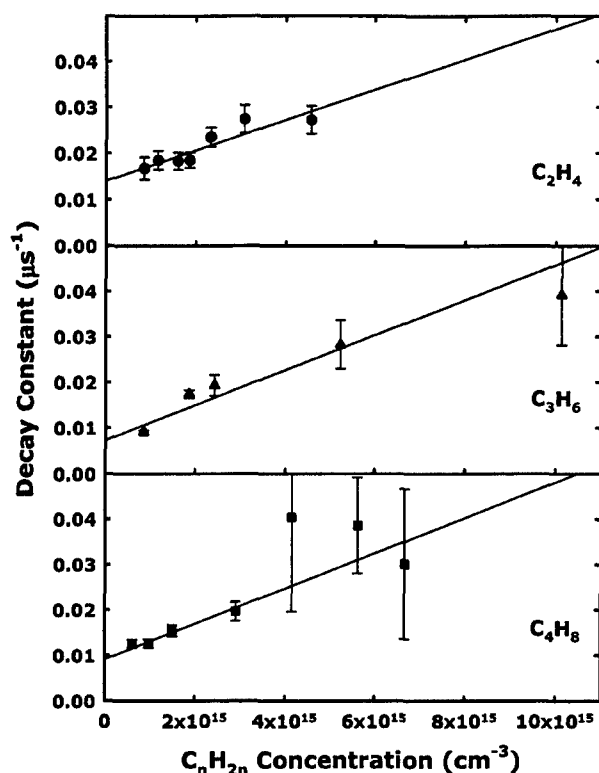


Figure 9. Best-fit exponential decay constants for quenching of the integrated CO₂ ν_3 emission (1900–2000 cm⁻¹) as a function of the C₂H₄, C₃H₆, and *n*-C₄H₈ concentration.

TABLE 3: Rate Constants k_Q for the Quenching of CO₂ Emission (1900–2000 cm⁻¹) by C₂H₄, C₃H₆, and *n*-C₄H₈, Compared to Relative Lennard-Jones Collision Frequencies

	k_Q (cm ³ s ⁻¹)	k_Q (relative)	$k_{\text{coll}}(\text{L-J})$ (relative)
C ₂ H ₄	$(3.3 \pm 0.8) \times 10^{-12}$	1.00	1.00
C ₃ H ₆	$(3.8 \pm 0.5) \times 10^{-12}$	1.15	1.03
<i>n</i> -C ₄ H ₈	$(4.2 \pm 0.7) \times 10^{-12}$	1.27	1.12

The emitting vibrational levels and energies can be approximately identified by using the known anharmonic and vibrational mode coupling constants of CO₂. Emission in the 1900–2000 cm⁻¹ region corresponds to roughly 15–19 quanta of energy in the ν_3 mode. Of course, fewer ν_3 quanta are excited if the exothermicity is partially channeled into the lower energy ν_1 and ν_2 modes. These ν_3 levels have associated term energies of 33 000–41 000 cm⁻¹, as much as 93% of the CO–O bond dissociation energy, $D_0 = 43\,980$ cm⁻¹.

The derived rate constants for the relaxation of the excited CO₂ by C₂H₄, C₃H₆, and *n*-C₄H₈ are given in Table 3. The values increase only modestly with increasing carbon chain length, with the quenching roughly 1% efficient based on a gas kinetic collision rate. The increase is similar to the estimated 12% increase in the collision rate calculated by using Lennard-Jones parameters derived from experimental second virial coefficients.^{35,36} The alkenes have C=C stretch frequencies (1623–1647 cm⁻¹)³⁴ that are as little as 250 cm⁻¹ lower in frequency than the high-energy CO₂ ν_3 vibrations, suggesting that V–V transfer could play a role in the relaxation process. Note that C₃H₆ and *n*-C₄H₈ have IR-active C=C stretch modes with nonzero transition dipole moments, unlike C₂H₄, which has a center of symmetry. However, the fact that the relaxation rate constants are not significantly larger for C₃H₆ and *n*-C₄H₈ implies that V–V transfer induced by long-range forces does not make a significant contribution to the quenching mechanism. Relaxation by SO₂ was found to be very inefficient ($<10^{-15}$

cm⁻³ s⁻¹), consistent with the lack of a vibrational mode frequency near those of highly excited CO₂.

4. Summary

A new experiment has been initiated to measure and characterize the IR emissions resulting from the interactions of O atoms with hydrocarbons. In an initial study, O atoms were prepared by photolyzing SO₂, then reacted with C₂H₄. The nascent fast O atoms are largely thermalized through collisions with Ar bath gas prior to reaction, resulting in O + C₂H₄ primary reaction and related secondary chemistry proceeding under thermal conditions. The resultant IR chemiluminescence signal was detected by using a step-scan FTIR spectrometer for simultaneous time- and frequency-dependent data collection. Emission has been observed from CO, CO₂, HCO, H₂CO, and other product species. Integrated radiance in the CO₂ ν_3 emission region has been correlated with reactant species partial pressures and laser fluence. A chemical kinetics model has been used to identify secondary chemistry responsible for the appearance of chemiluminescent CO and CO₂ and to characterize the partial pressure and fluence dependences. Rate constants for the relaxation of highly vibrationally excited CO₂ by C₂H₄, C₃H₆, and *n*-C₄H₈ have been determined, the values increasing only modestly with increasing alkene chain length.

Acknowledgment. This research was supported by the Air Force Office of Scientific Research under Task 2303ES/92VS04COR. This work was performed while K.J.C. held a National Research Council Research Associateship Award and G.D.D. an AFOSR Summer Faculty Fellowship, both at the Air Force Research Laboratory. E.S.H. performed this work under Contract F19628-98-C-0058 with the Air Force.

References and Notes

- (1) Hedin, A. E. *J. Geophys. Res.* **1991**, *96*, 1159.
- (2) Gardner, J. L.; Miller, S. M. *J. Chem. Phys.* **2004**, accepted for publication.
- (3) Linan, A.; Williams, F. A. *Fundamental Aspects of Combustion*; Oxford University Press: London, UK, 1993.
- (4) Schmoltner, A. M.; Chu, P. M.; Brudzynski, R. J.; Lee, Y. T. *J. Chem. Phys.* **1989**, *91*, 6926.
- (5) Abou-Zied, O. K.; McDonald, J. D. *J. Chem. Phys.* **1998**, *109*, 1293.
- (6) Morton, M. L.; Szpunar, D. E.; Butler, L. J. *J. Chem. Phys.* **2001**, *115*, 204.
- (7) Bley, U.; Dransfeld, P.; Himme, B.; Koch, M.; Temps, F.; Wagner, H. G. Primary products of the reaction between O(³P)-atoms and C₂H₄ studied with esr- and lmr-detection; Twenty-Second Symposium (International) on Combustion, 1988.
- (8) Endo, Y.; Tsuchiya, S.; Yamada, C.; Hirota, E. *J. Chem. Phys.* **1986**, *85*, 4446.
- (9) Su, H.; Bersohn, R. *J. Chem. Phys.* **2001**, *115*, 217.
- (10) Neyer, D. W.; Kable, S. H.; Loison, J.-C.; Houston, P. L.; Burak, I.; Goldfield, E. M. *J. Chem. Phys.* **1992**, *97*, 9036.
- (11) Neyer, D. W.; Luo, X.; Houston, P. L.; Burak, I. *J. Chem. Phys.* **1993**, *98*, 5095.
- (12) Neyer, D. W.; Luo, X.; Burak, I.; Houston, P. L. *J. Chem. Phys.* **1995**, *102*, 1645.
- (13) Keller, H.-M.; Schinke, R. *J. Chem. Soc., Faraday Trans.* **1997**, *93*, 879.
- (14) Keller, H.-M.; Floethmann, H.; Dobbyn, A. J.; Schinke, R.; Werner, H.-J.; Bauer, C.; Rosmus, P. *J. Chem. Phys.* **1996**, *105*, 4983.
- (15) Brandt-Pollmann, U.; Weiss, J.; Schinke, R. *J. Chem. Phys.* **2001**, *115*, 8876.
- (16) Werner, H.-J.; Bauer, C.; Rosmus, P.; Keller, H.-M.; Stumpf, M.; Schinke, R. *J. Chem. Phys.* **1995**, *102*, 3593.
- (17) Huang, Y.-L.; Gordon, R. J. *J. Chem. Phys.* **1990**, *93*, 868.
- (18) Kawasaki, M.; Sato, H. *Chem. Phys. Lett.* **1987**, *139*, 585.
- (19) Felder, P.; Effenhauser, C. S.; Haas, B. M.; Huber, J. R. *Chem. Phys. Lett.* **1988**, *148*, 417.
- (20) Freedman, A.; Yang, S.-C.; Bersohn, R. *J. Chem. Phys.* **1979**, *70*, 5313.
- (21) Fletcher, T. R.; Leone, S. R. *J. Chem. Phys.* **1988**, *88*, 4720.

- (22) Welsh, H. L.; Cumming, C.; Stansbury, E. J. *J. Opt. Soc. Am.* **1951**, *41*, 712.
- (23) Welsh, H. L.; Stansbury, E. J.; Romanko, J.; Feldman, T. J. *Opt. Soc. Am.* **1955**, *45*, 338.
- (24) Woodbridge, E. L.; Fletcher, T. R.; Leone, S. R. *J. Phys. Chem.* **1988**, *92*, 5387.
- (25) Jones, L. C., Jr.; Taylor, L. W. *Anal. Chem.* **1955**, *27*, 228.
- (26) Dodd, J. A.; Hwang, E. S.; Castle, K. J.; DeBoer, G. D. O + C_nH_{2n} products detected via IR emission. 2. O + C_nH_{2n} (n = 1–3), manuscript in preparation.
- (27) Cvetanovic, R. J. *J. Phys. Chem. Ref. Data* **1987**, *16*, 261.
- (28) Baulch, D. L.; Cobos, C. J.; Cox, R. A.; Frank, P.; Hayman, G.; Just, T.; Kerr, J. A.; Murrells, T.; Pilling, M. J.; Troe, J.; Walker, R. W.; Warnatz, J. *J. Phys. Chem. Ref. Data* **1994**, *23*, 847.
- (29) Matsumi, Y.; Shamsuddin, S. M.; Sato, Y.; Kawasaki, M. *J. Chem. Phys.* **1994**, *101*, 9610.
- (30) Min, Z.; Wong, T.-H.; Quandt, R.; Bersohn, R. *J. Phys. Chem. A* **1999**, *103*, 10451.
- (31) Min, Z.; Wong, T.-H.; Su, H.; Bersohn, R. *J. Phys. Chem. A* **2000**, *104*, 9941.
- (32) Quandt, R.; Min, Z.; Wang, X.; Bersohn, R. *J. Phys. Chem. A* **1998**, *102*, 60.
- (33) Su, H.; Bersohn, R. *J. Phys. Chem. A* **2001**, *105*, 9178.
- (34) Bozzelli, J. W. *J. Chem. Educ.* **2000**, *77*, 165.
- (35) Hirschfelder, J. O.; Curtiss, C. F.; Bird, R. B. *Molecular theory of gases and liquids*; John Wiley and Sons: New York, 1954.
- (36) Kaye, G. W. C.; Laby, T. H. *Tables of Physical and Chemical Constants*, 15th ed.; Longman: New York, 1986.